

Big Bang Nucleosynthesis: Reprise

Subir Sarkar

Department of Physics, 1 Keble Road, Oxford OX1 3NP, UK

Abstract. Recent observational and theoretical developments concerning the primordial synthesis of the light elements are reviewed, and the implications for dark matter mentioned.

1. Introduction

Why yet another review of big bang nucleosynthesis (BBN)? Given that the basic physics of the synthesis of the light elements D, ^3He , ^4He and ^7Li in the big bang was thoroughly discussed over 25 years ago [1, 2] it is natural to wonder why so many papers on the subject continue to appear on a regular basis. The reason for this is two-fold. First, as observational determinations of light element abundances have advanced, the situation has become *more* instead of less uncertain. In particular it has become apparent that inferring the primordial values of the abundances from contemporary observations is fraught with uncertainty, given our limited understanding of the chemical evolution of galaxies. Fortunately observers have risen to the challenge and developed sophisticated techniques to look further back into our past, at nearly pristine primordial material. However large discrepancies, most likely of a systematic nature, have subsequently emerged between different determinations, so the improvement in precision has not led to an increase in accuracy! Nevertheless this is a healthy development in that it has provided a refreshing perspective on the strong claims made in the past decade concerning the consistency of BBN predictions with the inferred primordial abundances, and on the stringent constraints thus inferred on new physics. The second development concerns recent efforts to improve the accuracy of the theoretical predictions of the abundances, and, just as important, to quantify the uncertainties. In this talk I will discuss these issues and summarize their implications for the dark matter problem and for new physics, viz. $N_\nu \neq 3$. Other recent reviews [3, 4, 5] may be consulted for a different perspective than mine [6, 7].

2. Theoretical Calculations

We now have excellent semi-analytic insights into the physics of BBN which enable the ${}^4\text{He}$ abundance to be calculated correctly to within $\sim 1 - 2\%$ [8] and the ‘left-over’ abundances of D, ${}^3\text{He}$, and ${}^7\text{Li}$ to be estimated to within a factor of $\sim 2 - 3$ [9]. However for precision work, and in particular, to determine the uncertainties, it is necessary to use the Wagoner computer code [2] which has been improved and updated with the latest values of the nuclear cross-sections and made freely available to the community [10, 11].

There have been two important developments on this front. First the rates for the weak interactions which determine the neutron-to-proton ratio have been carefully calculated beyond the Born approximation, with allowance for all zero and finite temperature radiative, Coulomb and finite (nucleon) mass corrections [12, 13]. With further allowance for finite temperature QED corrections to the equation of state of the plasma and the residual coupling of the neutrinos to the plasma during e^+e^- annihilation, the ${}^4\text{He}$ abundance has been computed with an accuracy of $\sim 0.4\%$ [12], where the dominant source of uncertainty comes from the present experimental determination of the neutron lifetime: $\tau_n = 885.3 \pm 2.0$ s [14]. This is an impressive feat and it is believed that all relevant physical processes have now been consistently taken into account.

The uncertainties in the abundances of the other light elements are of course considerably greater and are, moreover, correlated with each other. The standard practice has been to use the Monte Carlo method to sample the error distributions of the relevant reaction cross-sections which are then input into the numerical code, thus enabling well-defined confidence levels to be attached to the theoretically predicted abundances [15, 16]. However this is computationally expensive and, moreover, needs to be repeated each time any of the input parameters are changed or updated.¹ To overcome this handicap we have developed a method based on linear error propagation which requires the numerical code to be run just once to determine the covariance (or error) matrix; simple χ^2 statistics can then be used (rather than maximum likelihood methods as with Monte Carlo simulations) to determine e.g. the best-fit value of $\eta \equiv n_N/n_\gamma$, the nucleon-to-photon ratio [17]. This method has recently been extended to consider departures from the standard model, viz. an effective number of neutrinos N_ν during BBN different from 3, so that correlated limits on η and N_ν can be extracted for any given set of input abundances [18]. The results agree well, where comparison is possible, with similar exercises using the Monte Carlo plus maximum likelihood method [19, 20]. All the calculations have been encoded in a simple code which is available from a website [11].

¹ For example, it has recently been argued [21] that uncertainties in the cross-sections for some key nuclear reactions are in fact smaller than were estimated earlier [15].

The method is briefly as follows. First define the four relevant elemental abundances as $Y_2 \equiv \text{D}/\text{H}$, $Y_3 \equiv {}^3\text{He}/\text{H}$, $Y_7 \equiv {}^7\text{Li}/\text{H}$, and finally Y_4 as the *mass fraction* of ${}^4\text{He}$ (often termed Y_{P}). These depend both on the model parameters η and N_ν , and on a network of nuclear reactions R_k :

$$Y_i = Y_i(\eta, N_\nu, \dots; \{R_k\}) . \quad (1)$$

The rates for the 12 essential nuclear reactions which have to be considered plus their associated uncertainties have been discussed in detail [15] and we use these, apart from the updated value of the neutron lifetime [14]. Now for a small change of the input rate R_k ($R_k \rightarrow R_k + \delta R_k$), the corresponding deviation of the i -th elemental abundance ($Y_i \rightarrow Y_i + \delta Y_i$) as given by linear propagation reads

$$\delta Y_i(\eta) = Y_i(\eta) \sum_k \lambda_{ik}(\eta) \frac{\delta R_k}{R_k} , \quad (2)$$

where the functions $\lambda_{ik}(\eta)$ represent the logarithmic derivatives of Y_i with respect to R_k :

$$\lambda_{ik}(\eta) = \frac{\partial \ln Y_i(\eta)}{\partial \ln R_k(\eta)} . \quad (3)$$

In general, the deviations δY_i are correlated, since they all originate from the same set of reaction rate shifts $\{\delta R_k\}$. The global information is contained in the error matrix (also called covariance matrix) [22], which is a generalization of the “error vector” δY_i in eq. (2). In particular, the abundance error matrix $\sigma_{ij}^2(\eta)$ obtained by linearly propagating the input $\pm 1\sigma$ reaction rate uncertainties $\pm \Delta R_k$ to the output abundances Y_i reads:

$$\sigma_{ij}^2(\eta) = Y_i(\eta) Y_j(\eta) \sum_k \lambda_{ik}(\eta) \lambda_{jk}(\eta) \left(\frac{\Delta R_k}{R_k} \right)^2 . \quad (4)$$

This matrix completely defines the abundance uncertainties. In particular, the 1σ abundance errors σ_i of Y_i are given by the square roots of the diagonal elements,

$$\sigma_i(\eta) = \sqrt{\sigma_{ii}^2(\eta)} , \quad (5)$$

while the error correlations ρ_{ij} can be derived from eqs. (4,5) through the standard definition

$$\rho_{ij}(\eta) = \frac{\sigma_{ij}^2(\eta)}{\sigma_i(\eta) \sigma_j(\eta)} . \quad (6)$$

We have checked that the propagation of errors is indeed linear and then computed the error matrix above, finding good agreement with the results obtained by Monte Carlo [15, 16].

Next we must input the inferred values of the primordial abundances, $\overline{Y}_i \pm \overline{\sigma}_i$. Taking the errors $\overline{\sigma}_i$ in the determinations of different abundances \overline{Y}_i to be uncorrelated, the experimental squared error matrix $\overline{\sigma}_{ij}^2$ is simply

$$\overline{\sigma}_{ij}^2 = \delta_{ij} \overline{\sigma}_i \overline{\sigma}_j , \quad (7)$$

where δ_{ij} is Kronecker's delta. The total (experimental + theoretical) error matrix S_{ij}^2 is then obtained by summing the matrices in eqs. (4,7):

$$S_{ij}^2(\eta) = \sigma_{ij}^2(\eta) + \overline{\sigma}_{ij}^2 . \quad (8)$$

Its inverse defines the weight matrix $W_{ij}(\eta)$:

$$W_{ij}(\eta) = [S_{ij}^2(\eta)]^{-1} . \quad (9)$$

The χ^2 statistic associated with the difference between theoretical (Y_i) and observational (\overline{Y}_i) light element abundance determinations is then [22]:

$$\chi^2(\eta) = \sum_{ij} [Y_i(\eta) - \overline{Y}_i] \cdot W_{ij}(\eta) \cdot [Y_j(\eta) - \overline{Y}_j] . \quad (10)$$

Contours of equal χ^2 can then be used to set bounds on the parameters η and N_ν at selected confidence levels. For standard BBN we set $N_\nu = 3$ and minimization of the χ^2 then gives the most probable value of η , while the intervals defined by $\chi^2 = \chi_{\min}^2 + \Delta \chi^2$ give the likely ranges of η at the confidence level set by $\Delta \chi^2$.

Below we have provided a table of polynomial fits to the central values of the abundances, $Y_i = a_0 + a_1 x + a_2 x^2 + a_3 x^3 + a_4 x^4 + a_5 x^5$, with $x \equiv \log_{10}(\eta/10^{-10})$ in the range 0–1 [17]. The value of Y_4 from the Wagner code was corrected as described earlier [6] and is in excellent agreement with a subsequent precision calculation [12]. These fits, along with similar fits to the logarithmic derivatives $\lambda_{ik}(x)$ [17], have been encoded in a javascript program which plots the abundances with associated uncertainties and allows the corresponding values of η to be read off for a given input abundance [23]. We now proceed to discuss the observational situation.

	a_0	a_1	a_2	a_3	a_4	a_5
$Y_2 \times 10^3$	+0.4808	-1.8112	+3.2564	-3.3525	+1.8834	-0.4458
$Y_3 \times 10^5$	+3.4308	-6.1701	+8.1311	-9.7612	+7.7018	-2.5244
$Y_4 \times 10^1$	+2.2305	+0.5479	-0.6050	+0.6261	-0.3713	+0.0949
$Y_7 \times 10^9$	+0.5369	-2.8036	+7.6983	-12.571	+12.085	-3.8632

3. Observed Abundances

The abundances of the light elements synthesized in the big bang have been subsequently modified through chemical evolution of the astrophysical environments where they are measured [24]. The observational strategy then is to identify sites which have undergone as little chemical processing as possible and rely on empirical methods to infer the primordial abundance. For example, measurements of deuterium (D) can now be made in quasar absorption line systems (QAS) at high red shift; if there is a “ceiling” to the abundance in different QAS then it can be assumed to be the primordial value, since it is believed that there are no astrophysical sources of D. The helium (^4He) abundance is measured in H II regions in blue compact galaxies (BCGs) which have undergone very little star formation; its primordial value is inferred either by using the associated nitrogen or oxygen abundance to track the stellar production of helium, or by simply averaging over the most metal-poor objects [25]. (We do not consider ^3He which can undergo both creation and destruction in stars [24] and is thus unreliable for use as a cosmological probe.) Closer to home, the observed uniform abundance of lithium (^7Li) in the hottest and most metal-poor Pop II stars in our Galaxy is believed to reflect its primordial value [26].

However as remarked earlier, improvements in observational methods have made the situation more, instead of less, uncertain. Large discrepancies, of a systematic nature, have emerged between different observers who report, e.g., relatively ‘high’ [27, 28, 29] or ‘low’ [30] values of deuterium in different QAS, and ‘low’ [31, 32] or ‘high’ [33, 34] values of helium in BCG, using different data reduction methods. It has been argued that the Pop II lithium abundance [35, 36, 37] may in fact have been significantly depleted down from its primordial value [39, 40], with some observers arguing to the contrary [41].

Rather than take sides in this matter we instead consider several combinations of observational determinations, which cover a wide range of possibilities, in order to demonstrate our method and obtain illustrative best-fits for η and N_ν .

3.1. Deuterium

The first observations of D absorption due to a QAS at redshift $z = 3.32$ towards Q0014+813 suggested a relatively ‘high’ value of [27, 28]

$$\overline{Y}_2 = 1.9 \pm 0.4 \times 10^{-4}, \quad (11)$$

and was consistent with limits set in other QAS. However subsequent independent measurements in QAS at $z = 3.572$ towards Q1937-1009 and at

$z = 2.504$ towards Q1009+2956 found a much lower abundance of [30]

$$\overline{Y}_2 = 3.4 \pm 0.3 \times 10^{-5} . \quad (12)$$

More recently, observations of a QAS at $z = 0.701$ towards Q1718+4807 have also yielded a high abundance of [29]

$$\overline{Y}_2 = 3.3 \pm 1.2 \times 10^{-4} . \quad (13)$$

These discrepant measurements may result from spatial variations of the D abundance due to localized astrophysical processes [28] or due to inhomogeneous nucleosynthesis [42]. More prosaic explanations invoke systematic effects. For example, new data on the Q0014+813 system [43] reveal the presence of an ‘interloper’ hydrogen line contaminating the deuterium absorption feature. It has also been suggested [44] that the discordance between the ‘high’ and ‘low’ values may be considerably reduced if the analysis of the H+D profiles accounts for the correlated velocity field of bulk motion, i.e. mesoturbulence, rather than being based on multi-component microturbulent models. It is then found that a true primordial abundance of

$$\overline{Y}_2 = (3.5 - 5.2) \times 10^{-5} \quad (14)$$

is compatible simultaneously (at 95% C.L.) with the ‘low’ and ‘high’ values quoted above in eqs. (12,13) if the data on these objects is appropriately analysed. Whether this is indeed the correct explanation in all cases is however not clear. Obviously more measurements are needed and at the moment all the suggested values of the primordial deuterium abundance quoted above merit consideration.

3.2. Helium

The primordial helium abundance is found to be [32]

$$\overline{Y}_4 = 0.234 \pm 0.002 \pm 0.005 , \quad (15)$$

from linear regression to zero metallicity in a set of 62 BCGs, based largely on observations which gave a relatively ‘low’ value [31]. However using data on a sample of 27 BCGs from an independent survey, a significantly higher value of

$$\overline{Y}_4 = 0.243 \pm 0.003 , \quad (16)$$

has been derived from a new analysis which uses the helium lines themselves to self-consistently determine the physical conditions in the H II region [33] and specifically excludes those regions (with anomalously low He I line intensities) which are believed to be affected by underlying stellar absorption. In particular it has been demonstrated that there is strong

underlying stellar absorption in the NW component of I Zw 18, which was included in earlier analyses [31]. Excluding this, the average of the values found in the two most metal-poor BCGs, I Zw 18 and SBS 0335-052, is [34]

$$\overline{Y}_4 = 0.245 \pm 0.004 . \quad (17)$$

Again further work is needed to resolve the situation but we will consider both the ‘low’ and ‘high’ values for the primordial helium abundance.

3.3. Lithium

The controversy here concerns whether the observed approximately constant ‘Spite plateau’ in the abundance of ${}^7\text{Li}$ in Pop II stars in the halo reflects its true primordial value or has been depleted down from an initially higher abundance. There is agreement that the average value in the hottest and most metal-poor stars is about [35, 36]

$$\overline{Y}_7 = 1.6 \pm 0.36 \times 10^{-10} , \quad (18)$$

but there is dispute about whether there is significant scatter suggestive of some depletion mechanism, or a slight trend of decreasing ${}^7\text{Li}$ abundance with increasing metallicity suggestive of secondary cosmic ray production. A recent analysis based on 41 stars finds no evidence of any depletion or post-BBN creation and suggests a slightly higher primordial abundance [37],

$$\overline{Y}_7 = 1.73 \pm 0.21 \times 10^{-10} . \quad (19)$$

(The systematic error may have to be raised by $\sim 50\%$ to allow for the uncertainty in the oscillator strengths of the lithium lines [26].)

However there are hot, metal-poor Pop II stars which appear identical to those which define the ‘Spite plateau’ but which have *no* detectable ${}^7\text{Li}$ [35, 38], indicating that some depletion mechanism does exist. Recently it has been argued that the observed abundance has been depleted down from a primordial value of [45]

$$\overline{Y}_7 = 3.9 \pm 0.85 \times 10^{-10} , \quad (20)$$

the lower end of the range being set by the presence of the highly overdepleted halo stars and consistency with the ${}^7\text{Li}$ abundance in the Sun and in open clusters, while the upper end of the range is set by the observed dispersion about the ‘Spite plateau’ and the ${}^6\text{Li}/{}^7\text{Li}$ depletion ratio. A somewhat smaller depletion is suggested by other workers [40] who find a primordial abundance of $\overline{Y}_7 = 2.3 \pm 0.5 \times 10^{-10}$.

The implications of all these possibilities need study.

4. Implications for η and baryonic dark matter

Elsewhere [18] we have discussed various combinations of the above data sets and provided a handy computer programme [11] to enable the reader to consider other permutations/combinations. Here we will present results for just two possible (although mutually incompatible) selections of measurements which we name data set ‘‘A’’ and data set ‘‘B’’:

$$\text{Data set A : } \begin{cases} \overline{Y}_2 = 1.9 \pm 0.4 \times 10^{-4} , \\ \overline{Y}_4 = 0.234 \pm 0.0054 , \\ \overline{Y}_7 = 1.6 \pm 0.36 \times 10^{-10} ; \end{cases} \quad (21)$$

$$\text{Data set B : } \begin{cases} \overline{Y}_2 = 3.40 \pm 0.25 \times 10^{-5} , \\ \overline{Y}_4 = 0.243 \pm 0.003 , \\ \overline{Y}_7 = 1.73 \pm 0.21 \times 10^{-10} . \end{cases} \quad (22)$$

(In subsequent figures we also consider a slight variation of data set B in which we use eq. (17) instead of eq. (16) for the ${}^4\text{He}$ abundance.)

Figure 1 shows the theoretical predictions compared with the data. We calculate and minimize the χ^2 and obtain the 95% C.L. ranges allowed by each data set by cutting the curves at $\Delta\chi^2 = \chi^2 - \chi_{\min}^2 = 3.84$:

$$\text{Data set A : } \eta = 1.78_{-0.34}^{+0.54} \times 10^{-10}, \quad (23)$$

$$\text{Data set B : } \eta = 5.13_{-0.66}^{+0.72} \times 10^{-10}. \quad (24)$$

The range of η for data set A agrees very well with the 95% C.L. range obtained independently with the same input data but using the Monte Carlo plus maximum likelihood method [19]. However it is inconsistent with a further constraint on η coming from a recent analysis of the Ly α -‘‘forest’’ absorption lines in quasar spectra. The observed mean opacity of the lines requires some minimum amount of neutral hydrogen in the high redshift intergalactic medium, given a lower bound to the flux of ionizing radiation. Taking the latter from a conservative estimate of the integrated UV background due to quasars yields the constraint [46]

$$\eta > 3.4 \times 10^{-10} . \quad (25)$$

Using $\Omega_N h^2 \simeq \eta/2.73 \times 10^{-8}$ this corresponds to $\Omega_N > 0.0125h^{-2}$, where Ω_N is the density of nucleons in ratio to the critical density and h is the present Hubble parameter in units of $100 \text{ km s}^{-1} \text{ Mpc}^{-1}$.

Thus data set B is favoured by the Ly α -forest constraint. The implied nucleon density is significantly higher than the nucleonic matter in stars and X-ray emitting gas in groups and clusters today [47],

$$\Omega_N \equiv \frac{\rho_N}{\rho_c} \sim 0.0025h^{-1} + 0.0046h^{-1.5} , \quad (26)$$

implying that most of the nucleons are presently in some dark form.

Standard BBN predictions vs data (1σ errors)

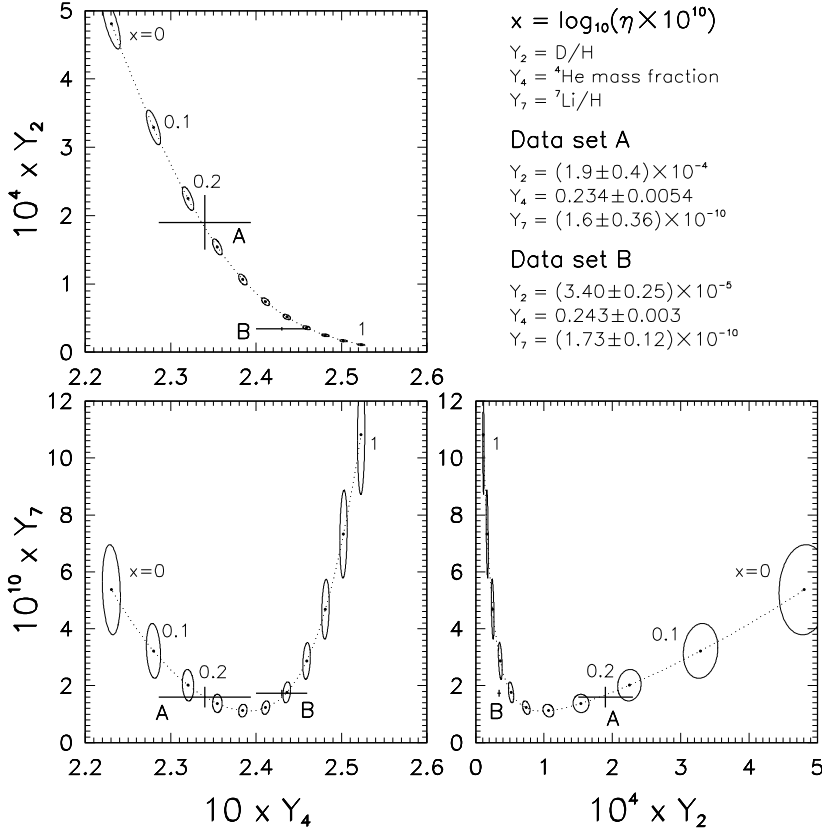


Figure 1. Standard BBN predictions (dotted lines) in the planes defined by the abundances Y_2 , Y_4 , and Y_7 [17]. The theoretical uncertainties are depicted as 1σ error ellipses at $x \equiv \log_{10}(\eta/10^{-10}) = 0, 0.1, 0.2, \dots, 1$. The crosses indicate the two observational data sets (with 1σ errors).

5. New Physics and the Possibility of $N_\nu \neq 3$

We should also take into account that the goodness of fit can be affected by a non-standard Hubble expansion rate during BBN, e.g. due to the presence of new neutrinos. Although the Standard Model contains only $N_\nu = 3$ weakly interacting massless neutrinos, the recent experimental evidence for neutrino oscillations [48] may require it to be extended to include new superweakly interacting massless (or very light) particles such

as singlet neutrinos or Majorons. These do not couple to the Z^0 vector boson and are therefore unconstrained by the precision studies of Z^0 decays which establish the number of $SU(2)_L$ doublet neutrino species to be [14]

$$N_\nu = 2.993 \pm 0.011 . \quad (27)$$

However, as was emphasized some time ago [49], such particles would boost the relativistic energy density, hence the expansion rate, during BBN, thus increasing the yield of ${}^4\text{He}$. This argument was quantified for new types of neutrinos and new superweakly interacting particles [50] in terms of a bound on the *equivalent number of massless neutrinos* present during nucleosynthesis:

$$N_\nu = 3 + f_{\text{B,F}} \sum_i \frac{g_i}{2} \left(\frac{T_i}{T_\nu} \right)^4 , \quad (28)$$

where g_i is the number of (interacting) helicity states, $f_{\text{B}} = 8/7$ (bosons) and $f_{\text{F}} = 1$ (fermions), and the ratio T_i/T_ν depends on the thermal history of the particle under consideration [51]. For example, $T_i/T_\nu \leq 0.465$ for a particle which decouples above the electroweak scale such as a singlet Majoron or a sterile neutrino. However the situation may be more complicated, e.g. if the sterile neutrino has large mixing with a left-handed doublet species, it can be brought into equilibrium through (matter-enhanced) oscillations in the early universe, making $T_i/T_\nu \simeq 1$ [52]. Moreover such oscillations can generate an asymmetry between ν_e and $\bar{\nu}_e$, thus directly affecting neutron-proton interconversions and the resultant yield of ${}^4\text{He}$ [53]. This can be quantified in terms of the *effective* value of N_ν parametrizing the expansion rate during BBN, which may well be below 3! Similarly, non-trivial changes in N_ν can be induced by the decays [54] or annihilations [55] of massive neutrinos (into e.g. Majorons), so it is clear that it is a sensitive probe of new physics.

The values of N_ν and η are correlated since the effect of a faster expansion rate can be compensated for by the effect of a smaller nucleon density. Indeed increasingly stringent lower bounds on η inferred from assumed upper limits to the primordial deuterium abundance (which were deduced from chemical evolution arguments) have been used to set increasingly stringent upper bounds on N_ν . These have ranged from 4 downwards [56], culminating in one below 3 which precipitated the so-called ‘‘crisis’’ for standard BBN [57], and was interpreted as requiring new physics. However as cautioned before [58], there are large systematic uncertainties in such constraints on N_ν which are sensitive to our limited understanding of galactic chemical evolution. Moreover it has been emphasized [16] that the procedure used earlier [56] to bound N_ν was statistically inconsistent since, e.g., correlations between the different elemental abundances were not taken into account. This can of course be addressed by the Monte

Carlo method, using which it was shown [59] that the *conservative* observational limits on the primordial abundances of D, ${}^4\text{He}$ and ${}^7\text{Li}$ allow $N_\nu \leq 4.53$ (95% C.L.), significantly less restrictive than earlier estimates. However because the Monte Carlo method is computationally expensive and the exercise needs to be redone e.g. whenever the input abundances change, it would clearly be advantageous to extend our linear error propagation approach to include N_ν as a parameter.

This is, in principle, straightforward, since it simply requires recalculation of the functions Y_i and λ_{ik} at the chosen value of N_ν . Since it would be impractical to use extensive tables of polynomial coefficients, we have devised some formulae which, to good accuracy, relate the calculations for arbitrary values of N_ν to the standard case $N_\nu = 3$, thus reducing the numerical task dramatically [18].

As is known from previous work [9], the synthesized elemental abundances D/H, ${}^3\text{He}/\text{H}$, and ${}^7\text{Li}/\text{H}$ (i.e., Y_2 , Y_3 , and Y_7 in our notation) are given to a good approximation by the quasi-fixed points of the corresponding rate equations, which formally read

$$\frac{dY_i}{dt} \propto \eta \sum_{+,-} Y \times Y \times \langle \sigma v \rangle_T, \quad (29)$$

where the sum runs over the relevant source (+) and sink (-) terms, and $\langle \sigma v \rangle_T$ is the thermally-averaged reaction cross section. Since the temperature of the universe evolves as $dT/dt \propto -T^3 \sqrt{g_\star}$, with the number of relativistic degrees of freedom, $g_\star = 2 + (7/4)(4/11)^{4/3} N_\nu$ (following e^+e^- annihilation), the above equation can be rewritten as

$$\frac{dY_i}{dT} \propto -\frac{\eta}{g_\star^{1/2}} T^{-3} \sum_{+,-} Y \times Y \times \langle \sigma v \rangle_T, \quad (30)$$

which shows that Y_2 , Y_3 , and Y_7 depend on η and N_ν essentially through the combination $\eta/g_\star^{1/2}$. Thus the calculated abundances Y_2 , Y_3 , and Y_7 (as well as their logarithmic derivatives λ_{ik}) should be approximately constant for

$$\log \eta - \frac{1}{2} \log g_\star = \text{constant}, \quad (31)$$

as we have verified numerically.

This suggests that the values of Y_i and of λ_{ik} for $N_\nu = 3 + \Delta N_\nu$ can be related to the case $N_\nu = 3$ through an appropriate shift in x :

$$Y_i(x, 3 + \Delta N_\nu) \simeq Y_i(x + c_i \Delta N_\nu, 3), \quad (32)$$

$$\lambda_{ik}(x, 3 + \Delta N_\nu) \simeq \lambda_{ik}(x + c_i \Delta N_\nu, 3), \quad (33)$$

where the coefficient c_i is estimated to be ~ -0.03 from eq. (31) (at least for small ΔN_ν). In order to obtain a satisfactory accuracy in the whole

range $(x, N_\nu) \in [0, 1] \times [1, 5]$, we in fact allow upto a second-order variation in ΔN_ν , and for a rescaling factor of the Y_i 's. As regards the ${}^4\text{He}$ abundance, a semi-analytical approximation [8] also suggests a relation between x and N_ν similar to eq. (31), although with different coefficients, and indeed functional relations of the kind above work well also in this case. However, in order to achieve higher accuracy and, in particular, to match exactly the result of the recent precision calculation of Y_4 which includes all finite temperature and finite density corrections [12], we also allow for a rescaling factor for the λ_{4k} 's. All these calculations have been embedded in a compact Fortran programme available from a website [11], which allows easy extraction of joint fits to x and N_ν for a given set of elemental abundances, without having to run the full BBN code, and with no significant loss in accuracy. We now proceed to discuss these fits.

6. Joint fits to η and N_ν

Figure 2 shows the abundances for various N_ν compared for illustration with data set A. While there is consistency between theory and data for $x \sim 0.2 - 0.4$ and $N_\nu = 3$, for $N_\nu = 2$ ($N_\nu = 4$) the Y_2 data prefer values of x lower (higher) than the Y_4 data. Therefore, we expect that a global fit will favor values of (x, N_ν) close to $(0.3, 3)$. Similarly, a fit to data set B should favour values of $(x, N_\nu) \sim (0.7, 3)$ as seen in figure 3.

To quantify this we show in figure 4 the results of joint fits using the abundances of data set A. The abundances Y_2 , Y_4 , and Y_7 are used separately (upper panels), in combinations of two (middle panels), and all together, without and with the $\text{Ly}\alpha$ -forest constraint² on η (lower panels). In this way the relative weight of each piece of data in the global fit can be understood at glance. The three C.L. curves (solid, thick solid, and dashed) are defined by $\chi^2 - \chi_{\min}^2 = 2.3, 6.2, \text{ and } 11.8$, respectively, corresponding to 68.3%, 95.4%, and 99.7% C.L. for two degrees of freedom (η and N_ν), i.e., to the probability intervals often designated as 1, 2, and 3 standard deviation limits. The χ^2 is minimized for each combination of Y_i , but the actual value of χ_{\min}^2 (and the best-fit point) is shown only for the relevant global combination $Y_2 + Y_4 + Y_7(+\text{Ly}\alpha)$. For this data set, the helium and deuterium abundances dominate the fit, as can be seen by comparing the combinations $Y_2 + Y_4$ and $Y_2 + Y_4 + Y_7$. The preferred values of x are relatively low, and the preferred values of N_ν range between 2 and 4. Although the fit is excellent, the low value of x is in conflict with the $\text{Ly}\alpha$ -forest constraint on η , as indicated by the increase of χ_{\min}^2 from 0.02 to 8.89.

² This bound is not well-defined statistically but we can parametrize it for example through a penalty function $\chi_{\text{Ly}\alpha}^2(\eta) = 2.7 \times (3.4 \times 10^{-10}/\eta)^2$ which can be added to the χ^2 derived from our fit to the elemental abundances.

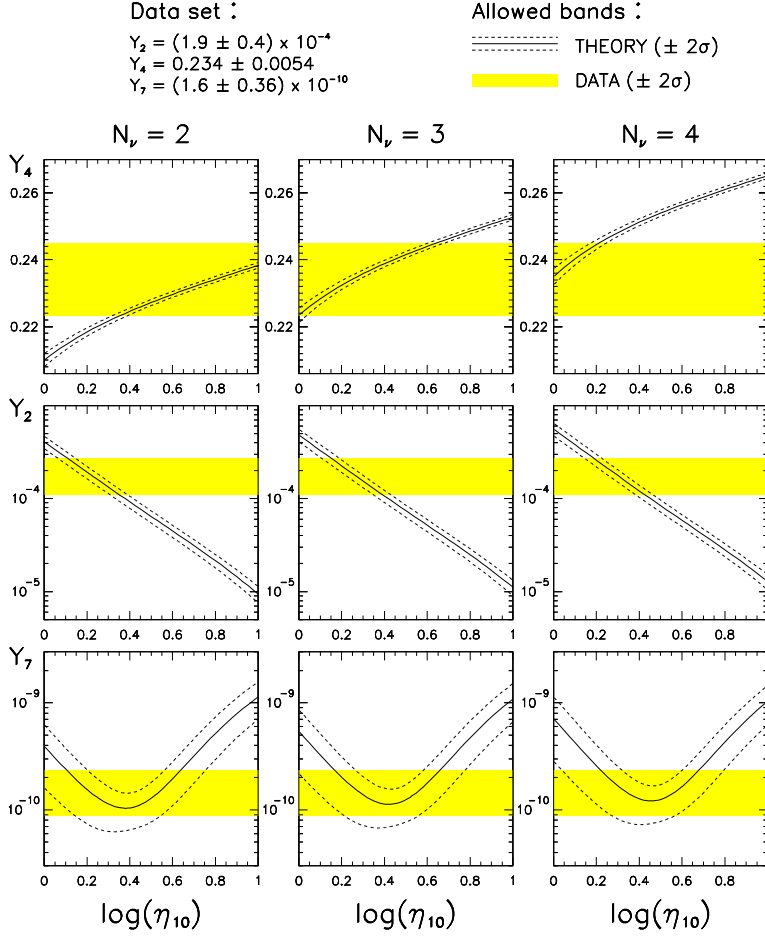


Figure 2. Primordial abundances Y_4 (${}^4\text{He}$ mass fraction) Y_2 (D/H) and Y_7 (${}^7\text{Li}/\text{H}$), for $N_\nu = 2, 3,$ and 4 . Solid and dashed curves represent the theoretical central values and the $\pm 2\sigma$ bands, respectively. The grey areas represent the $\pm 2\sigma$ experimental bands for the data set A [18].

As shown in figure 5 there is no such problem with data set B which favors high values of x because of the ‘low’ deuterium abundance. The combination of $Y_2 + Y_7$ isolates, at high x , a narrow strip which depends mildly on N_ν . The inclusion of Y_4 selects the central part of such strip, corresponding to N_ν between 2 and 4. As in figure 4, the combination $Y_4 + Y_7$ does not appear to be very constraining. The overall fit to $Y_2 + Y_4 + Y_7$

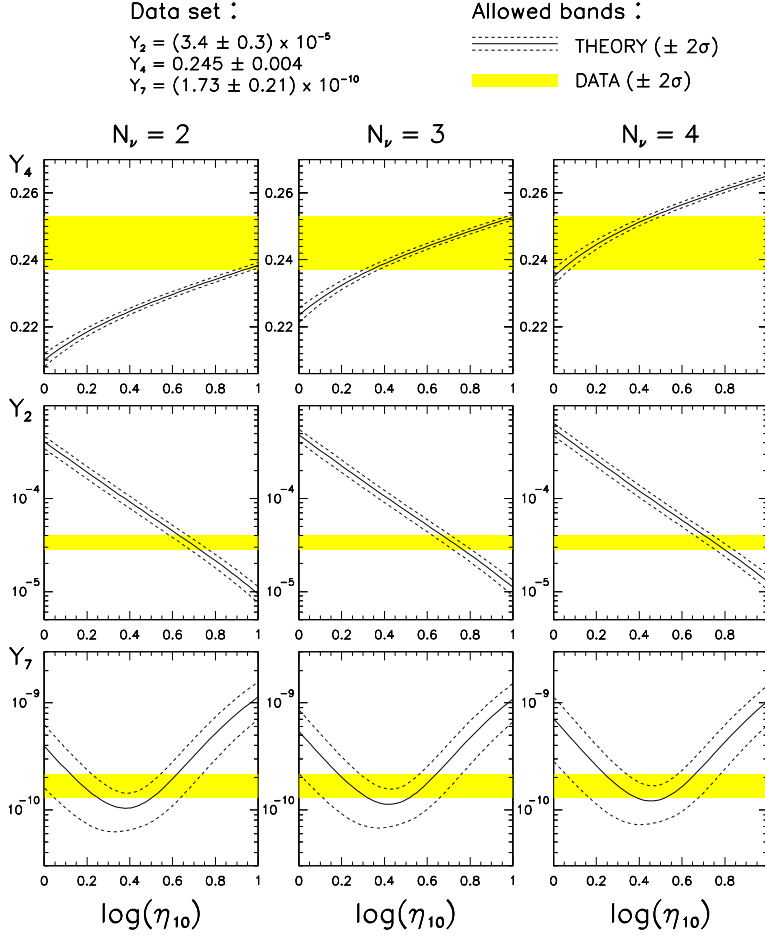


Figure 3. Same as in figure 2, but for data set B [18].

is acceptable but not particularly good, mainly because Y_2 and Y_7 are only marginally compatible at high x . On the other hand, the $Y_2 + Y_4 + Y_7$ bounds are quite consistent with the Ly α -forest constraint.

Elsewhere [18] we have presented results for other possible combinations of input abundances. As shown in figure 6 (cf. [20]), one can also consider orthogonal combinations to those above, e.g. ‘high’ deuterium *and* ‘high’ helium, or ‘low’ deuterium *and* ‘low’ helium. The latter combination implies $N_\nu \sim 2$, thus creating the so-called “crisis” for standard nucleosynthesis [57]. Conversely, the former combination suggests $N_\nu \sim 4$, which would

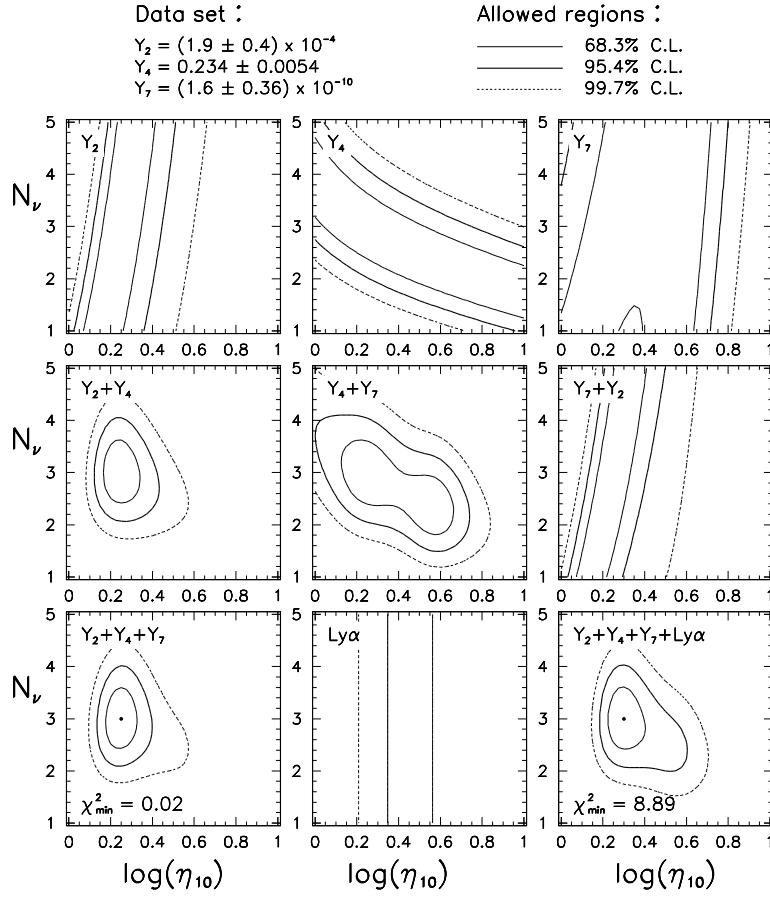


Figure 4. Joint fits to $x = \log(\eta_{10})$ and N_ν using the abundances of data set A [18]. The abundances Y_2 , Y_4 , and Y_7 are used separately (upper panels), in combinations of two (middle panels), and all together, without and with the Ly α -forest constraint on η (lower panels).

also constitute evidence for new physics. Allowing for depletion of the primordial lithium abundance to its Pop II value, relaxes the upper bound on N_ν further, as was noted earlier [59].

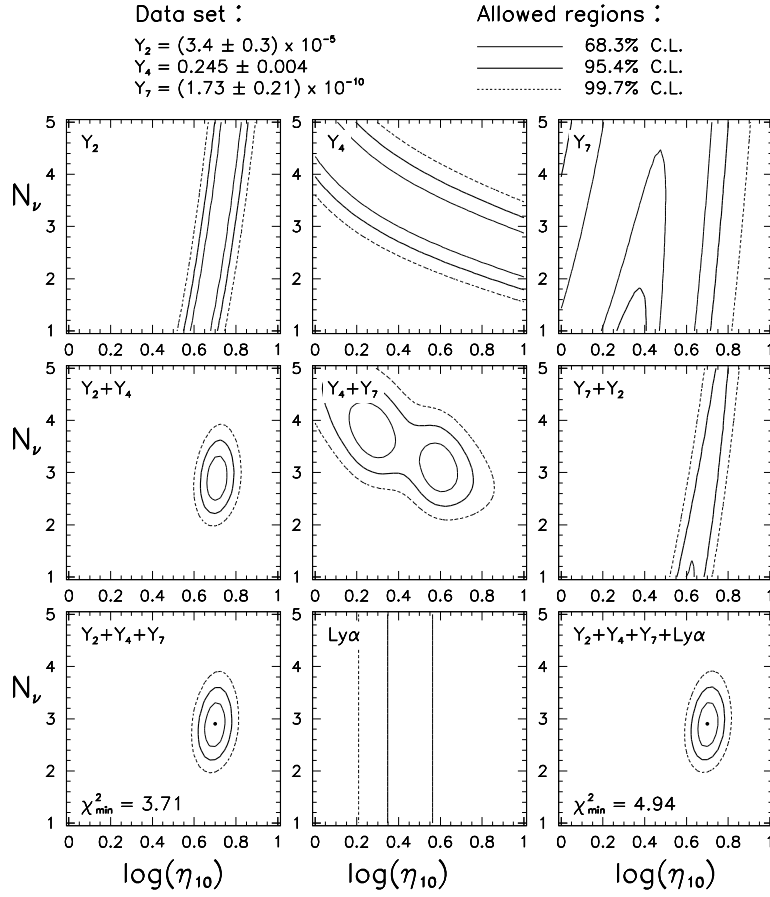


Figure 5. Same as in Fig. 4, but for the data set B [18].

7. Conclusions

It is clear from the above discussion that the present observational data on the primordial elemental abundances are not as yet sufficiently stable to derive firm bounds on η and N_ν . Different and arguably equally acceptable choices for the input data sets lead to very different predictions for η , and to relatively loose constraints on N_ν in the range 2 to 4 at the 95% C.L. Thus it may be premature to quote restrictive bounds based on some particular combination of the observations, until the discrepancies between different

deuterium and helium

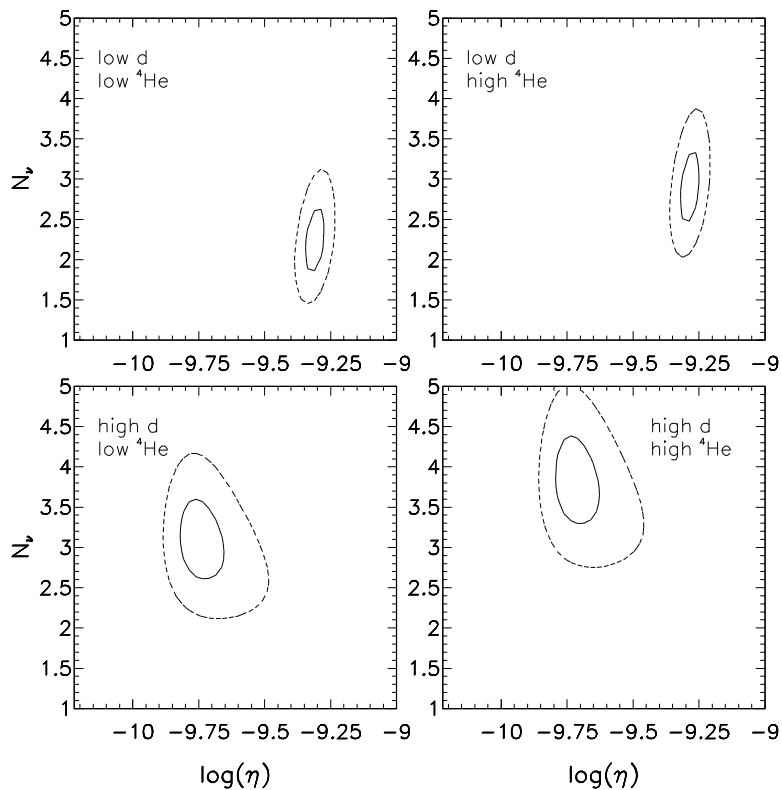


Figure 6. The 68% (solid) and 95% (dotted) likelihood contours for the number of neutrino species and the nucleon-to-photon ratio, for all four combinations of the ‘high’ and ‘low’ deuterium and helium abundance measurements in data sets A and B.

estimates are satisfactorily resolved. Our method of analysis provides the reader with an easy-to-use technique [11] to recalculate the best-fit values as the observational situation evolves further.

In order to improve the theoretical predictions further it is necessary to know the nuclear reaction rates better. To determine which reaction is largely responsible for the uncertainty in a particular elemental abundance (for any given nucleon density) is clearly important in this regard. In our approach this can be easily determined by “perturbing” the values of the

Big Bang Nucleosynthesis – Error Components
at $\eta = 1.78 \times 10^{-10}$

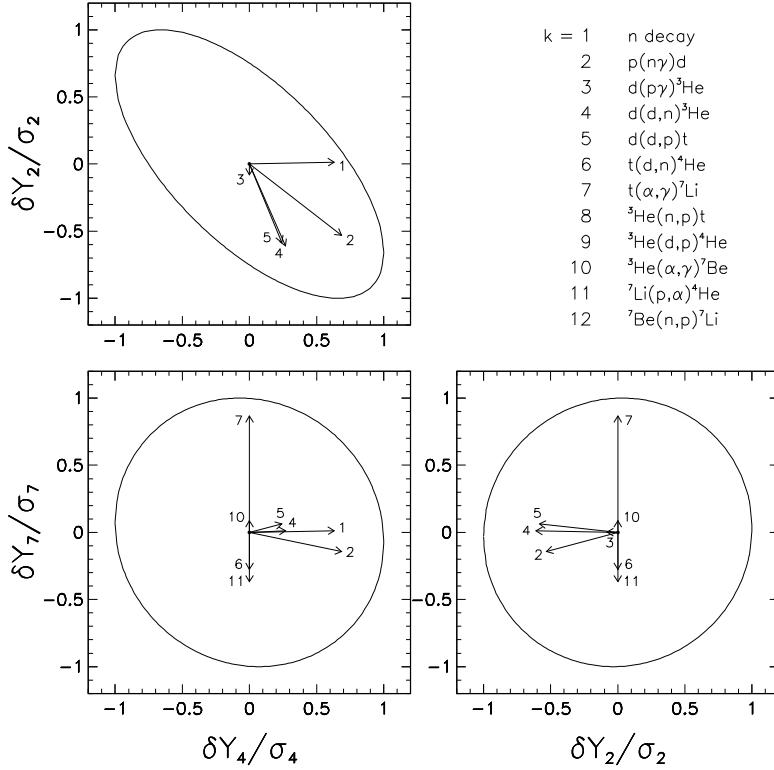


Figure 7. Individual contributions of different reaction rates R_k to the uncertainties in Y_2 , Y_4 , and Y_7 , normalized to the corresponding total errors σ_2 , σ_4 , and σ_7 , for $\eta = 1.78 \times 10^{-10}$, the best-fit value for data set A [17]. Each arrow corresponds to the shift δY_i induced by a $+1\sigma$ shift of R_k . Some small error components have not been plotted.

input reaction rates and observing their effect on the predicted abundances, namely one can study the contribution to the total uncertainty σ_i of Y_i induced by a $+1\sigma$ shift of R_k :

$$R_k \rightarrow R_k + \Delta R_k \implies Y_i \rightarrow Y_i + \delta Y_i . \quad (34)$$

We choose two particular values of η , 1.78×10^{-10} and 5.13×10^{-10} , corresponding to the best-fit values for data sets A and B respectively and show in figures 7 and 8 the deviations δY_i (normalized to the total error σ_i)

Big Bang Nucleosynthesis – Error Components
at $\eta = 5.13 \times 10^{-10}$

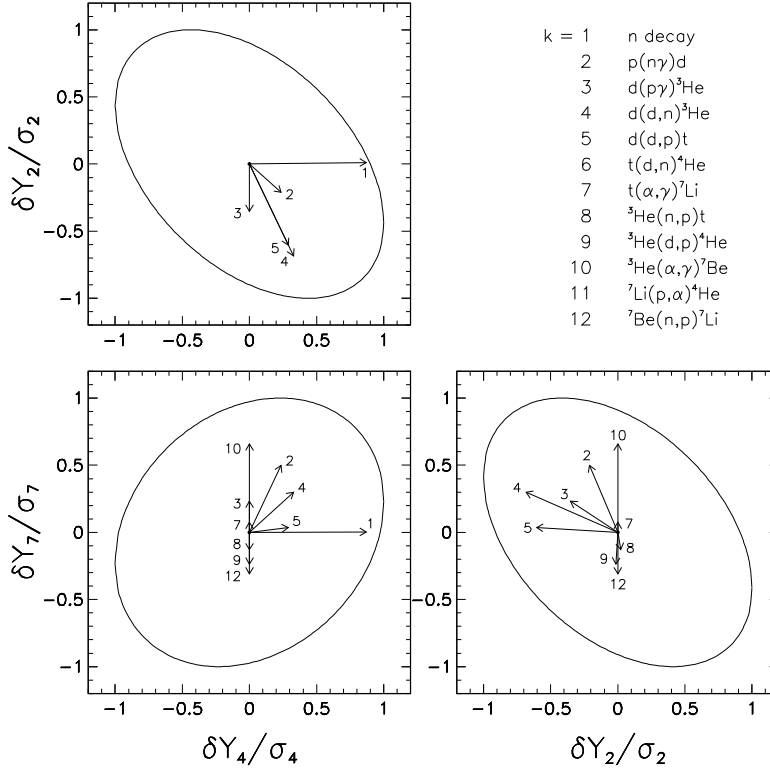


Figure 8. Same as in figure 7, but for $\eta = 5.13 \times 10^{-10}$, the best-fit value for data set B [17].

induced by $+1\sigma$ shifts in the R_k 's, plotted in the same set of planes as used for figure 1. The 1σ error ellipses shown in these figures are obtained by combining the deviation vectors $\delta Y_i/\sigma_i$ in an uncorrelated manner. Several interesting conclusions can be drawn from this exercise. As expected, the uncertainty in the weak interaction rate R_1 has the greatest impact on Y_4 for the high value of η (figure 8), since essentially all neutrons end up being bound in ^4He . However at the lower value of η (figure 7), the uncertainty in R_2 — the “deuterium bottleneck” — plays an equally important role as R_1 in determining Y_4 because nuclear burning is less complete here than at high η . Similarly with reference to the reaction rates R_7 , $R_{10} - R_{12}$ which synthesize ^7Li , at low η it is the competition between R_7 and R_{11}

which largely determines Y_7 , while at high η it is the competition between R_{10} and R_{12} . The anticorrelation between Y_4 and Y_2 is driven mainly by R_2 at low η and, to a lesser extent, by R_4 and R_5 , while the reverse is the case at high η . The anticorrelation between Y_4 and Y_7 at low η is also basically driven by R_2 , while the correlation at high η is due to both R_2 and R_4 . Thus we have a direct visual basis for assessing in what direction the output abundances Y_i are pulled by possible changes in the input cross sections R_k . This should be helpful in determining experimental strategies to determine key reaction rates more precisely.

However one might ask what would happen if these discrepancies remain? We have already noted the importance of an independent constraint on η (from the Ly α -forest) in discriminating between different options. However, given the many assumptions which go into the argument [46], this constraint is rather uncertain at present. Fortunately it should be possible in the near future to independently determine η to within $\sim 5\%$ through measurements of the angular anisotropy of the cosmic microwave background (CMB) on small angular scales [60], in particular with data from the all-sky surveyors MAP and PLANCK [61]. Such observations will also provide a precision measure of the relativistic particle content of the primordial plasma. Hopefully the primordial abundance of ^4He would have stabilized by then, thus providing, in conjunction with the above measurements, a reliable probe of a wide variety of new physics and astrophysics which can affect nucleosynthesis (for recent work see [62, 63, 64, 65, 66, 67]).

Acknowledgments

It is a pleasure to thank Laura Baudis and Hans Klapdor-Kleingrothaus for organizing this enjoyable meeting, and my collaborators on BBN, Eligio Lisi and Francesco Villante, for allowing me to present our unpublished results.

References

- [1] Wagoner R V, Fowler W A and Hoyle F 1967 *Astrophys. J.* **148** 3
- [2] Wagoner R V 1973 *Astrophys. J.* **179** 343
- [3] Schramm D N and Turner M S 1998 *Rev. Mod. Phys.* **70** 303
- [4] Steigman G 1998 astro-ph/9803055
- [5] Olive K A 1999 astro-ph/9901231
- [6] Sarkar S 1996 *Rep. Prog. Phys.* **59** 1493
- [7] Sarkar S 1997 *Dark Matter in Astro- and Particle Physics*, ed H V Klapdor-Kleingrothaus and Y Ramachers (Singapore: World Scientific) p 235

- [8] Bernstein J A, Brown L S and Feinberg G 1989 *Rev. Mod. Phys.* **61** 25
- [9] Esmailzadeh R, Starkman G D and Dimopoulos S 1991 *Astrophys. J.* **378** 504
- [10] Kawano L 1992 Fermilab-Pub-92/04-A (unpublished)
- [11] <http://www-thphys.physics.ox.ac.uk/users/SubirSarkar/bbn.html>
- [12] Lopez R E and Turner M S 1998 astro-ph/9807279
- [13] Esposito S, Mangano G, Miele G and Pisanti O 1999 *Nucl. Phys.* B**540** 3
- [14] Caso C *et al* 1998 *Eur. J. Phys.* C**3** 1
- [15] Smith M S, Kawano L and Malaney R A 1993 *Astrophys. J. Suppl.* **85** 219
- [16] Kernan P and Krauss L M 1994 *Phys. Rev. Lett.* **72** 3309
Krauss L M and Kernan P 1995 *Phys. Lett.* **347** 347
- [17] Fiorentini G, Lisi E, Sarkar S and Villante F L 1998 *Phys. Rev.* D**58** 063506
- [18] Lisi E, Sarkar S and Villante F L 1999 hep-ph/9901404
- [19] Olive K A and Thomas D 1997 *Astropart. Phys.* **7** 27
- [20] Holtman E, Kawasaki M, Kohri K and Moroi T 1998 hep-ph/9805405.
- [21] Burles S, Nollett K M, Truran J N and Turner M S 1999 astro-ph/9901157
- [22] Eadie W T, Drijard D, James F E, Roos M and Sadoulet B 1971 *Statistical Methods in Experimental Physics* (Amsterdam: North Holland)
- [23] <http://www.astro.washington.edu/mendoza/java/bbn>
(will move to <http://www.astro.washington.edu/bbn/>)
- [24] Pagel B E J 1997 *Nucleosynthesis and the Chemical Evolution of Galaxies* (Cambridge: Cambridge University Press)
- [25] Hogan C 1998 *Sp. Sci. Rev.* **84** 127
- [26] Molaro P 1997 *From Quantum Fluctuations to Cosmological Structures*, ASP Conf. Ser. **126** 103; private communication
- [27] Songaila A, Cowie L L, Hogan C J and Rugers M 1994 *Nature* **368** 599
Carswell R F, Rauch M, Weymann R J, Cooke A J and Webb J K 1994
Mon. Not. R. Astr. Soc. **268** L1
- [28] Rugers M and Hogan C J 1996 *Astron. J.* **111** 2135
- [29] Webb J K, Carswell R F, Lanzetta K M, Ferlet R, Lemoine M and Vidal-Madjar A 1997 *Nature* **388** 250
Tytler D, Burles S, Lu L, Fan X-M, Wolfe A and Savage B D 1998 astro-ph/9810217
- [30] Tytler D, Fan X-M and Burles S 1996 *Nature* **381** 207
Burles S and Tytler D 1998 *Astrophys. J.* **499** 699; **507** 732; *Sp. Sci. Rev.* **84** 65
- [31] Pagel B E J, Simonson E A, Terlevich R J and Edmunds M G 1992 *Mon. Not. R. Astr. Soc.* **255** 325
Olive K A and Steigman G 1995 *Astrophys. J. Suppl.* **97** 49

- [32] Olive K A, Steigman G and Skillman E D 1997 *Astrophys. J.* **483** 788
- [33] Izotov Y I, Thuan T X and Lipovetsky V A 1994 *Astrophys. J.* **435** 647;
1997 *Astrophys. J. Suppl.* **108** 1
- [34] Izotov Y I and Thuan T X 1998 *Astrophys. J.* **497** 227, **500**, 188
- [35] Thorburn J A 1994 *Astrophys. J.* **421** 318
- [36] Molaro P, Primas F and Bonifacio P 1995 *Astron. Astrophys.* **295** L47
- [37] Bonifacio P and Molaro P 1997 *Mon. Not. Roy. Astron. Soc.* **285** 847
- [38] Ryan S G, Norris J E and Beers T C 1998 *Astrophys. J.* **506** 892
- [39] Pinsonneault M H, Deliyannis C P and Demarque P 1992 *Astrophys. J. Suppl.* **78** 179
- [40] Vauclair S and Charbonnel C 1995 *Astron. Astrophys.* **295** 715; 1998 *Astrophys. J.* **502** 372
- [41] Bonifacio P and Molaro M 1998 *Astrophys. J. Lett.* **500** L175
- [42] Jedamzik K and Fuller G M 1996 *Astrophys. J.* **483** 560
- [43] Burles S, Kirkman D and Tytler D 1996 astro-ph/9612121
- [44] Levshakov S A, Kegel W H and Takahara F 1998 *Astrophys. J.* **499** L1
Levshakov S A, Tytler D and Burles S 1998 astro-ph/9812114
- [45] Pinsonneault M H, Walker T P, Steigman G and Narayanan V K 1998 astro-ph/9803073
- [46] Weinberg D H, Miralda-Escudé J, Hernquist L and Katz N 1997 *Astrophys. J.* **490** 564
- [47] Persic M and Salucci P 1992 *Mon. Not. R. Astr. Soc.* **258** 14p
Fukugita M, Hogan C J and Peebles P J E 1998 *Astrophys. J.* **503** 518
- [48] Conrad J 1998 hep-ex/9811009
- [49] Hoyle F and Tayler R J 1964 *Nature* **203** 1108
Peebles P J E 1966 *Phys. Rev. Lett.* **16** 411
Shvartsman V F 1969 *JETP Lett.* **9** 184
- [50] Steigman G, Schramm D N and Gunn J 1977 *Phys. Lett.* **66B** 202
Steigman G, Olive K A and Schramm D N 1979 *Phys. Rev. Lett.* **43** 239
- [51] Olive K A, Schramm D N and Steigman G 1981 *Nucl. Phys.* **B180** 497
- [52] Enqvist K, Kainulainen K and Thomson M 1992 *Nucl. Phys.* **B373** 498
- [53] Kirilova D P and Chizhov M V 1998 *Nucl. Phys.* **B534** 447
Foot R and Volkas R R 1997 *Phys. Rev.* **D55** 5147
- [54] Dolgov A D, Hansen S H, Pastor S and Semikoz D V 1998 hep-ph/9809598
Hannestad S 1998 *Phys. Rev.* **D57** 2213
Kawasaki M, Kohri K and Sato K 1998 *Phys. Lett.* **B430** 132
- [55] Dolgov A D, Pastor S, Romão J C and Valle J W F 1997 *Nucl. Phys.* **B496**

- [56] Yang J, Turner M S, Steigman G, Schramm D N and Olive K A 1984 *Astrophys. J.* **281** 493
 Steigman G, Olive K A, Schramm D N and Turner M S 1986 *Phys. Lett.* **B176** 33
 Olive K A, Schramm D N, Steigman G and Walker T P 1990 *Phys. Lett.* **B236** 454
 Walker T P, Steigman G, Schramm D N, Olive K A and Kang H-S 1991 *Astrophys. J.* **376** 51
- [57] Hata N, Scherrer R J, Steigman G, Thomas D, Walker T P, Bludman S and Langacker P 1995 *Phys. Rev. Lett.* **75** 3977
- [58] Ellis J, Enqvist K, Nanopoulos D V and Sarkar S 1986 *Phys. Lett.* **B167** 457
- [59] Kernan P J and Sarkar S 1996 *Phys. Rev.* **D54** R3681
- [60] Knox L 1995 *Phys. Rev.* **D52** 4307
 Jungman G, Kamionkowski M, Kosowski A and Spergel D N 1996 *Phys. Rev.* **D54** 1332
 Zaldarriaga M, Spergel D N and Seljak U 1997 *Astrophys. J.* **488** 1
 Bond J R, Efstathiou G and Tegmark M 1997 *Mon. Not. R. Astron. Soc.* **291** L33
- [61] MAP: <http://map.gsfc.nasa.gov/>
 PLANCK: <http://astro.estec.esa.nl/SA-general/Projects/Planck/>
- [62] Bell N F, Foot R and Volkas R R 1998 *Phys. Rev.* **D58** 105010
- [63] Damour T and Pichon B 1998 astro-ph/9807176
- [64] Gherghetta T, Giudice G F and Riotto A 1998 hep-ph/9808401
- [65] Kainulainen K, Kurki-Suonio H and Sihvola E 1998 astro-ph/9807098
- [66] Mohapatra R N and Teplitz V L 1998 *Phys. Rev. Lett.* **81** 3079
- [67] Rehm J B and Jedamzik K 1998 *Phys. Rev. Lett.* **81** 3307